

Krzysztof Boryczko · Witold Dzwinel · David A. Yuen

Dynamical clustering of red blood cells in capillary vessels

Received: 22 July 2002 / Accepted: 16 October 2002 / Published online: 16 January 2003
© Springer-Verlag 2003

Abstract We have modeled the dynamics of a 3-D system consisting of red blood cells (RBCs), plasma and capillary walls using a discrete-particle approach. The blood cells and capillary walls are composed of a mesh of particles interacting with harmonic forces between nearest neighbors. We employ classical mechanics to mimic the elastic properties of RBCs with a biconcave disk composed of a mesh of spring-like particles. The fluid particle method allows for modeling the plasma as a particle ensemble, where each particle represents a collective unit of fluid, which is defined by its mass, moment of inertia, translational and angular momenta. Realistic behavior of blood cells is modeled by considering RBCs and plasma flowing through capillaries of various shapes. Three types of vessels are employed: a pipe with a choking point, a curved vessel and bifurcating capillaries. There is a strong tendency to produce RBC clusters in capillaries. The choking points and other irregularities in geometry influence both the flow and RBC shapes, considerably increasing the clotting effect. We also discuss other clotting factors coming from the physical properties of blood, such as the viscosity of the plasma and the elasticity of the RBCs. Modeling has been carried out with adequate resolution by using 1 to 10 million particles. Discrete particle simulations open a new pathway for modeling the dynamics of complex, viscoelastic fluids at the microscale, where both liquid and solid phases are treated with discrete particles.

Electronic Supplementary Material Supplementary material is available for this article if you access the article at <http://dx.doi.org/10.1007/s00894-002-0105-x>. A link in the frame on the left on that page takes you directly to the supplementary material.

K. Boryczko · W. Dzwinel
AGH Institute of Computer Science,
al. Mickiewicza 30, 30-059 Kraków, Poland

D. A. Yuen (✉)
Minnesota Supercomputing Institute,
University of Minnesota, MN, 55455 USA
e-mail: davey@krissy.geo.umn.edu

Keywords Blood flow · Capillaries · Clustering · Discrete-particle model · Fluid-particle model · Computer simulation

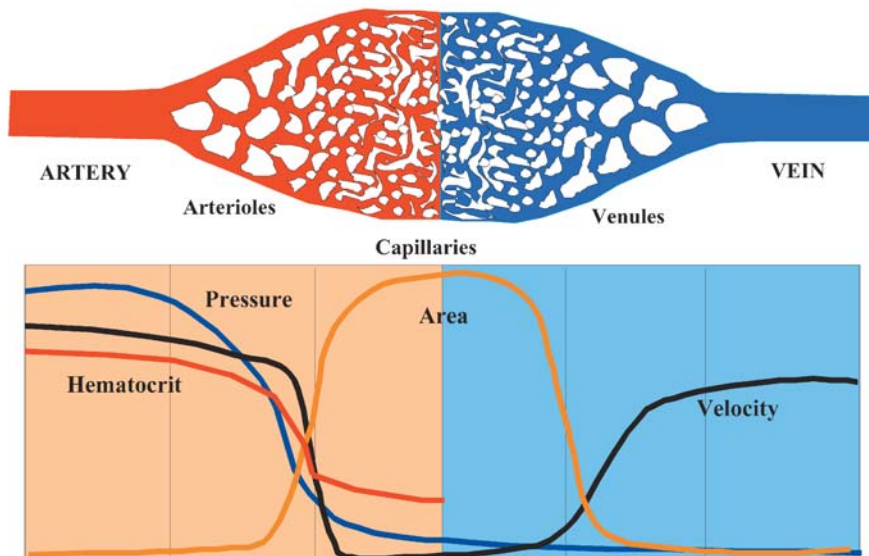
Introduction

Blood flow in microscopic capillaries with diameters on the order of the red blood cell (RBC) size represents a composite system with a sharp interface between liquid and solid phases. In this spatial scale, the RBCs represent the phase volume with distinct elastic properties. In contrast to the macroscale, where blood can be regarded as a continuous medium, at the microscopic scale blood flow can be viewed as the collective motion of an ensemble of microscopically interacting discrete particles.

Clustering of RBCs is a very important and vital biological process, [1, 2, 3, 4, 5] which influences the rheological properties of blood and may lead to severe cardiovascular problems, such as anemia, ischemia, angina, thrombosis and stroke. Many processes contributing to RBC coagulation have different origins. [1,6] Some of them represent very important immunological mechanisms, preventing the loss of blood from the system when blood vessels are cut or damaged. The clotting process is accomplished by the solidification of blood. Breakage of the lining of a vessel exposes the collagen proteins from the connective tissue to blood. This initiates three separate, but overlapping, hemostatic mechanisms: (1) RBC clustering; (2) the formation of a platelet plug; and (3) the production of a web of fibrin proteins around the platelet plug.

Clotting is irreversible, leading to the production of a thrombus, [1] which is carried away by flow after healing of the vessel. The thrombus is formed by an aggregation of blood components, primarily platelets and fibrin with the entrapment of cellular elements, frequently causing vascular obstruction at the point of its formation. Thromboses are prone to occur at sites where blood flow is sluggish. This type of slow flow or ischemia induces activated clotting factors to accumulate instead of being swept away by the blood flow.

Fig. 1 Changes in blood pressure, hematocrit, velocity and the area of the arteries, capillaries and veins of the multi-resolution circulatory system



One of the principal factors responsible for clotting and thrombosis is a clustering process of RBCs called aggregation. [2] The aggregates can have various structures, mostly chaotic and shapeless but sometimes taking on the appearance of a stacked pile of coins. These formations have been named rouleaux. When the number of cells in a rouleaux becomes reasonably large (>10), cross links between rouleaux can be formed, resulting in an extended network. According to the hypothesis formulated in, [7] aggregation/disaggregation play a very important role in providing a mechanism for controlling microvascular flow resistance. This mechanism is particularly important both for production of artificial blood and for control of blood circulation by the introduction of artificial blood substitutes into the vascular system. [8, 9]

Many experimental studies have been performed to investigate the mechanisms of red cell aggregation/disaggregation [1, 2, 9, 10, 11] and its influence on blood rheology. However, up to now, many questions remain unanswered. In order to investigate the role of aggregation/disaggregation in regulation of microvascular flow resistance, the aggregation mechanism should first be explained. Currently, two hypotheses are considered: the bridging mechanism and the depletion layer hypothesis. A reliable computational model simulating blood flow in capillary vessels should be formulated to verify these hypotheses. A basic problem in constructing this type of model comes from the diversified multiple spatio-temporal scales in which the blood clustering occurs.

Figure 1 shows the multi-resolutional hierarchy of the circulatory system. In the largest, arteries and veins having diameters on the order of a 10^{-2} m, blood pressure is about 10 kPa. In the smallest capillaries with diameters of 10^{-5} m the pressure drops to 1 kPa. Macroscopic vessels represent only a small fraction of the circulatory system, although the largest veins contain 50% of blood. The vascular tissue is made of microscopic capillary channels. There are about 10^{10} blood vessels whose diameters are comparable with the dimensions of the

RBCs, i.e., $5\text{--}10\ \mu\text{m}$. [12, 13] Therefore, the majority of defects in the circulatory blood system occurs in capillary vessels, where blood flows less vigorously than in larger macroscopic arteries and arterioles. These defects can become very dangerous if they occur over a large area and in vital parts of the organism, e.g., in the brain or eye. Bleeding over a vast capillary area is very feasible under extreme conditions such as: multiple g -acceleration exerted on jet pilots, or extremely low viscosity of blood caused by drugs or alcohol.

Most computer models of blood are motivated by fluid dynamic factors in the development of arterial diseases in large and medium vessels of the circulatory system. [14, 15] A common mathematical description of the blood flow treats blood as a homogeneous fluid and uses the full three-dimensional, time-dependent, incompressible Navier–Stokes equations for non-Newtonian fluids. [16] Blood rheology can be described by an appropriate shear-thinning model (e.g., by the Casson constitutive equations [1]) or can be based on experimental viscosity data. [2]

In contrast to the macroscale, at scales on the order of the red blood cell size, i.e., $10\ \mu\text{m}$, blood cannot be regarded physically as a liquid. Rather, it is a highly complex suspension of chemically and electrostatically active cells suspended in an electrolytic fluid with active proteins and organic substances. In this spatial scale the RBCs stand for the phase volume with elastic properties while the rest of the blood (plasma, platelets, enzymes, the network of insoluble fibrin molecules and other compounds) represents a colloidal suspension or a collective unit of fluid. In contrast to macroscopic simulations employing the traditional tools from computational fluid dynamics, in the microscopic scales the blood flow can be seen as a collective motion of an ensemble of interacting discrete objects. As shown in, [17] in small capillaries we do not observe homogeneous fluid flow but rather the motion of the RBCs lubricated by the rest of the colloidal suspension.

We present here a formal computational model of blood at the microscopic scale based on the discrete-particle paradigm with simple rules. [18] We demonstrate that the dynamics of a blood system, consisting of the RBCs, colloidal phase and the capillary walls, can be modeled successfully by using the discrete-particle approach. [19, 20] For the RBCs and capillary walls, we have constructed a 3-D mesh of particles interacting via harmonic forces with their nearest neighbors. We have simulated the plasma suspension by using fluid particles. The fluid particle model (FPM) [21] allows for modeling the colloidal mixture as a particle ensemble, where each particle represents an aggregation of small fluid droplets. The FPM method is similar in spirit to dissipative particle dynamics (DPD) – a technique recently introduced in modeling of complex fluids. [22, 23, 24, 25, 26, 27, 28, 29] The modeling has been carried out in three dimensions involving up to ten million particles for various geometries of the vessels, blood cells elasticity, and RBC shapes. We visualize the large-scale simulations both as detailed zoomed-in snapshots and as movies. Finally, we discuss and summarize the results.

Numerical model

In large arteries with a diameter more than two orders of magnitude greater than the size of an RBC, blood can be considered as a homogeneous fluid. Therefore, classical computational fluid dynamics can be used for modeling the blood flow in the macroscale (see e.g. Quarteroni, *SIAM News*, 2001 [30] and [31, 32, 33]). Mechanical properties of blood are usually described by a constitutive equation constructed on the basis of experimental viscometric data. The derivation of such an equation is nontrivial. It is indeed a very challenging task to take into account the complex boundary conditions associated with various geometries of blood vessels and elastic interactions between vessel wall and blood flow, modeling the realistic hydrodynamic behavior of blood in macroscopic vessels.

Feedback dynamics between microscopic flow and aggregation microstructures in capillary vessels require a completely different modeling approach. Formation of RBC clusters in the microscale cannot be simulated by classical computational fluid dynamics. Blood dynamics in the microscale must be studied as a two-phase, *non-homogeneous* fluid.

At the most elementary level, blood can be broken down into four main constituent parts: RBCs (erythrocytes), white blood cells (leukocytes), platelets, and the suspending plasma. The phase volume (hematocrit) can be quite variable, but is normally in the range 30–55% in larger arteries and drops to 10–15% in capillaries. Platelets occupy about 2% of the total blood volume, and white blood cells approximately 0.5%. Plasma is the fluid portion of blood.

We have made the following simplifications in the model:

1. RBCs are considered to be the phase volume with their own distinct elastic properties.
2. The rest of the blood (plasma, platelets, enzymes, the network of insoluble fibrin molecules and other components) is represented by a uniform colloidal suspension.
3. The blood flows in capillaries endowed with elastic walls.

While the number of constituent parts of the vascular system is currently limited, other components of blood, including artificial blood substitutes, can be added readily in a similar manner.

In capillary channels, it is necessary to consider all of the interactions between blood constituents, including tight interactions between the RBCs and the capillary walls. For modeling such an arrangement of interacting objects, we propose a discrete-particle model in which all the objects are made of mutually interacting elementary primitive [19, 20] particles, which evolve in time according to prescribed rules of motion governed by intermolecular forces.

Dynamical modeling of discrete particles – particle mesh and fluid particles

In macroscopic models, microscopic phenomena, such as interactions between cells resulting from depletion and electrostatic forces, chemical reactions, and large density fluctuations in plasma solution, are not present or are averaged out. Therefore, formation of RBC clusters cannot be modeled by integrating the equations of classical hydrodynamics numerically by using, e.g., finite element methods or finite differences. In the capillaries, RBCs must be treated as individual solid and elastic “objects” of circular biconcave shape. Consequently, blood in the microscale must be regarded as a two-phase, *nonhomogeneous* fluid consisting of a liquid plasma phase and deformable blood cells. These two phases are made of discrete particles.

These particles have several attributes such as mass m_i , moment of inertia \mathbf{I}_i , position \mathbf{r}_i , both translational \mathbf{v}_i and angular $\boldsymbol{\omega}_i$ velocities, type of force and others. Unlike molecular dynamics, a collision operator is used in the fluid particle model. Two particles i and j interact with each other by a collision operator Ψ_{ij} defined as a sum of constituent forces, whose parameters depend on the type of interacting particles. The forces can be central and/or noncentral. We use a two-body, short-ranged collision operator Ψ_{ij} with noncentral forces of the following form:

$$\Psi_{ij} = \sum_{\text{Type}} \mathbf{F}_{\text{Type}}(\mathbf{r}_{ij}, \mathbf{v}_{ij}, \boldsymbol{\omega}_{ij}) \cdot [\theta(\mathbf{r}_{ij}) - \theta(\mathbf{r}_{ij} - R_{\text{cut}})] \quad (1)$$

The summation runs through all types of forces, $\theta(\cdot)$ is a Heaviside step function and R_{cut} is the cut-off radius. The size of a particle can be defined by the value of R_{cut} the radius of interactions, or more precisely by the radius of the hard-core component of the force. Because the in-

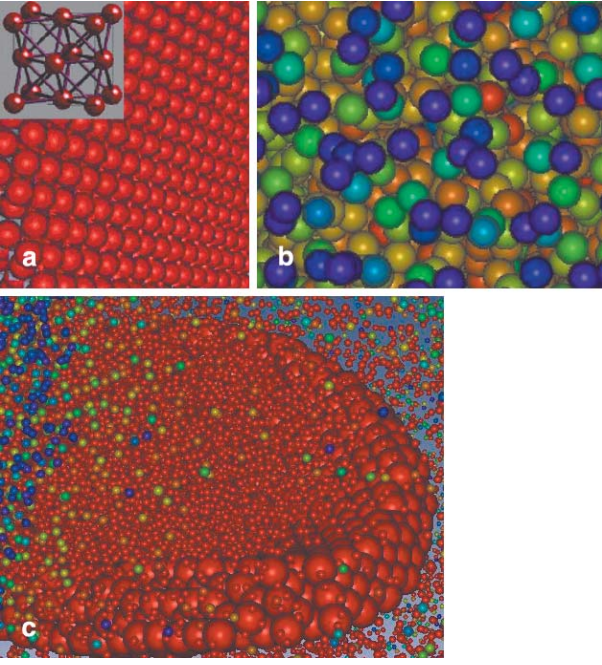


Fig. 2 Particles constrained on an fcc grid used for modeling. **a** The solid objects. **b** Particle fluid. **c** The composite solid–fluid structure taken together

teractions can be noncentral, the temporal evolution of the particle ensemble obeys the Newtonian equations of motion with rotational components:

$$\dot{\mathbf{v}}_i = \frac{1}{m} \sum_{i \neq j} \Psi_{ij} \quad (2)$$

$$\dot{\mathbf{r}}_i = \mathbf{v}_i \quad (3)$$

$$\dot{\boldsymbol{\omega}} = \frac{1}{I} \sum_{i \neq j} \mathbf{N}_{ij} \quad (4)$$

where the torques in Eq. (4) are given by:

$$\mathbf{N}_{ij} = -\frac{1}{2} \mathbf{r}_{ij} \times \Psi_{ij} \quad (5)$$

In our model there are two types of particle:

- *Solid particles* – the “pieces of matter” defining nodes of the elastic grid, as shown in Fig. 2a. They will represent the solid components of the vascular system, i.e., the vessel walls and RBCs.
- *Fluid particles* – representing portions of the colloidal suspension “chunks of fluid suspension” shown in Fig. 2b.

Both types of particles represent abstract objects in physical space, unlike the particles in molecular dynamics, where they represent actual atoms or molecules.

The definition of the collision operator is the principal factor that distinguishes solid and fluid particles. The “solid particles” are the compounds of larger objects with distinct shape, such as RBCs and the capillary walls. These objects are made of particles, whose initial positions are arranged – for simplicity of modeling – in

a face centered cubic (fcc) mesh. For cohesion the particles are coupled together by a harmonic potential with a mesh of particles on springs. We have assumed that the particles interact only with an invariant list of neighbors. This guarantees both that the objects will possess elastic properties and that the interparticle forces will be calculated efficiently.

The collision operator, defining the nature of the fluid particle, is of a different nature from the collision operator describing the solid particle. Similarly, as the solid particles stand for the “pieces of matter”, the fluid particles represent the “droplets of fluid”. In contrast to the mesh of particles on springs, the ensembles of fluid particles form shapeless structures (as shown in Fig. 2b) and have a variable number of neighbors within their interaction radius.

We assume in Fig. 2c that there are three different types of interactions: solid–solid, fluid–fluid and solid–fluid, and that we can couple together the two types of particle models, which can simulate a complex mixture with a sharp solid–fluid interface. The main problem, however, consists in a proper matching of the unknown collision operators to realistic physical properties of the system.

Red blood cells

The RBCs in a human vascular system are biconcave discs with dimensions 7–8 μm diameter, 2.5 μm thick at the edge and 1 μm at the center. They can be envisaged as soft bags containing hemoglobin. [1] A membrane provides the cell with its shape, strength and flexibility. It consists of a lipid bilayer supported by an extensive filament-like protein network, which is called the cytoskeleton. A number of proteins anchor the cytoskeleton to the lipid bilayer. These proteins also provide binding sites for glycolytic enzymes that endow the RBC with its negative surface charge. The mechanical properties of the individual blood cell produce various types of RBCs’ collective behavior, which influence the entire blood system considerably. [34]

We have assumed that the RBC is made of a mesh with particles on springs, as shown in Fig. 3, which models the cytoskeleton network. The particle i interacts with particles j in its closest neighborhood [35] by a conservative elastic force \mathbf{F}_{ij}^C where:

$$\mathbf{F}_{ij}^C = \chi \cdot (|r_{ij}| - a_{ij}) \mathbf{e}_{ij} \quad (6)$$

where χ defines the elasticity of the RBC and a_{ij} is the distance from a particle i to its nearest neighbor in equilibrium. The value of a_{ij} depends on the position of the neighboring particle for the initial conditions. For the fcc mesh and for only the first layer of neighbors the value of $a_{ij}=1$. Besides the conservative force, the collision operator for solid particles includes an additional dissipative force, which is a vector between particles i and j :

$$\mathbf{F}_{ij}^T = -\gamma \cdot m \hat{\mathbf{T}}_{ij} \circ \mathbf{v}_{ij} \quad (7)$$

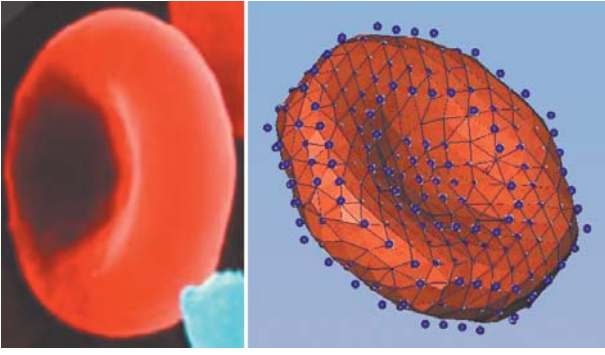


Fig. 3 A microscopic picture of RBC (left) and its 3-D DPM (right). Only surface particles are visible

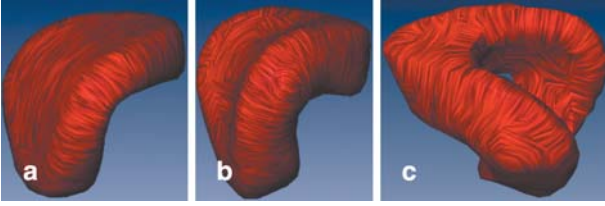


Fig. 4 The bent deflection for the three RBC models: (a) flat, (b) dual concavity and (c) discs with holes under the same load. The lines on the surface of RBC reveal the nature of vector field associated with the maximum curvature

where $\hat{\mathbf{T}}_{ij}$ is a tensor defined as follows:

$$\hat{\mathbf{T}}_{ij} = B(r_{ij}) \mathbf{e}_{ij} \mathbf{e}_{ij} \quad (8)$$

and γ is a dissipation factor, $B(r)$ a weighting function, $\mathbf{e}_{ij} = \mathbf{r}_{ij} / r_{ij}$.

The dissipative term prevents RBCs from breaking-up due to the collisions with the fast particles. Although the realistic RBC structure and its mesh model are different, the basic elastic properties of the model can be matched to the real blood cell by using mechanical principles.

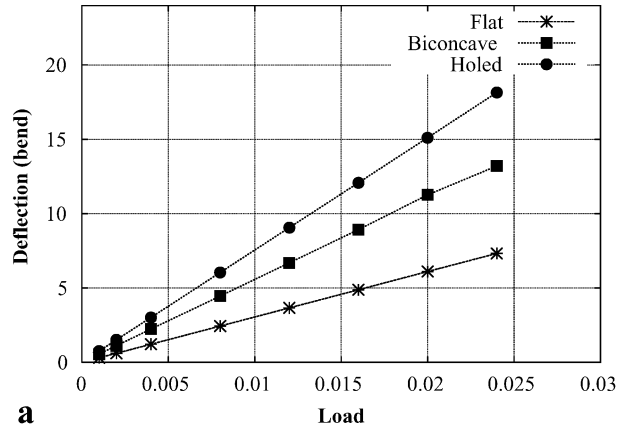
Let us consider a single RBC defined as a system of constrained nodes, the i th particle interacting with the j th particle with a force vector \mathbf{F}_{ik} . Initially, the system is in equilibrium. In Fig. 4a–c we consider two interacting particles i and k , whose positions \mathbf{r}_i and \mathbf{r}_k were changed due to interactions by $\mathbf{u}_i = \{u_i, v_i, w_i\}$ and $\mathbf{u}_k = \{u_k, v_k, w_k\}$ to $\mathbf{r}'_i, \mathbf{r}'_k$, respectively. The force \mathbf{F}_{ik} takes on the following value:

$$\mathbf{F}_{ik} = \frac{\varepsilon}{r_{ik}^3} \cdot (\mathbf{r}_i - \mathbf{r}_k) \circ (\mathbf{u}_i - \mathbf{u}_k) \cdot (\mathbf{r}_i - \mathbf{r}_k) \quad (9)$$

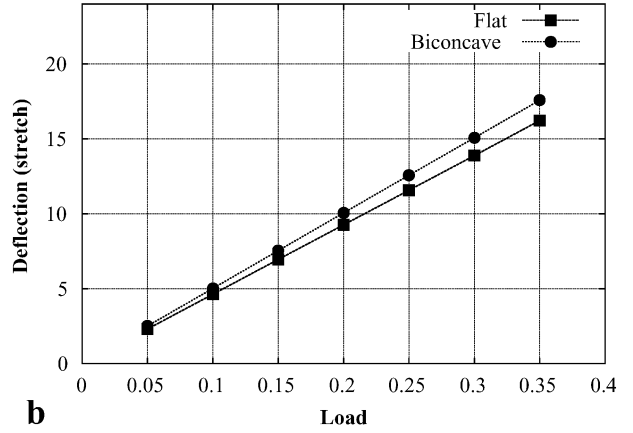
where ε is the absolute value of the accumulated strain. If the number of nearest neighbors of particle i is equal to N_i and the number of external forces \mathbf{P} acting on the particle i is equal to M , we obtain a set of linear equations:

$$\sum_{k=1}^{N_i} \frac{\varepsilon}{r_{ik}^3} \cdot (\mathbf{r}_i - \mathbf{r}_k) \circ (\mathbf{u}_i - \mathbf{u}_k) \cdot (\mathbf{r}_i - \mathbf{r}_k) - \sum_{m=1}^M \mathbf{P}_{im} = \mathbf{0} \quad (10)$$

from which \mathbf{u}_i can be easily computed for a given static load \mathbf{P} . We have investigated the bend and stretch deflec-



a



b

Fig. 5 The value of deflection response for the (a) bending and (b) stretching of flat and biconcave discs

tions of the RBC surface as a function of static load for the three RBC shapes: flat, biconcave and holed discs. The three shapes under the same load are shown in Fig. 4.

The linear characteristics compared in Fig. 5a,b differ from the nonlinear, mechanical properties of real blood cells. [1, 34] However, on the basis of the data displayed in Fig. 6 we can match elastic properties of the cell model to the system parameters and allow the cells to withstand large shear forces during their passage through the narrow capillaries. In Fig. 5 we show that the biconcave discs have a distinctly greater elasticity than the flat discs. The RBCs with holes perform even better but they represent cells that are characteristic of some blood diseases and are more relevant in producing clots. [1]

Capillary walls

Capillaries form a long network and are thin-walled blood vessels in which gas exchange occurs. In the capillary, the wall is only one cell layer thick. Capillaries are concentrated into capillary beds. Some capillaries have small pores between the cells of the capillary wall, allowing the materials to permeate through the capillaries

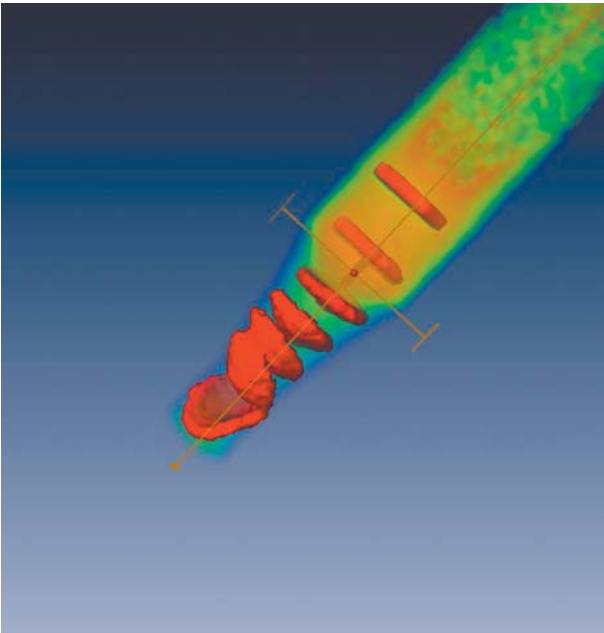


Fig. 6 RBC deformation modeled at a choking point

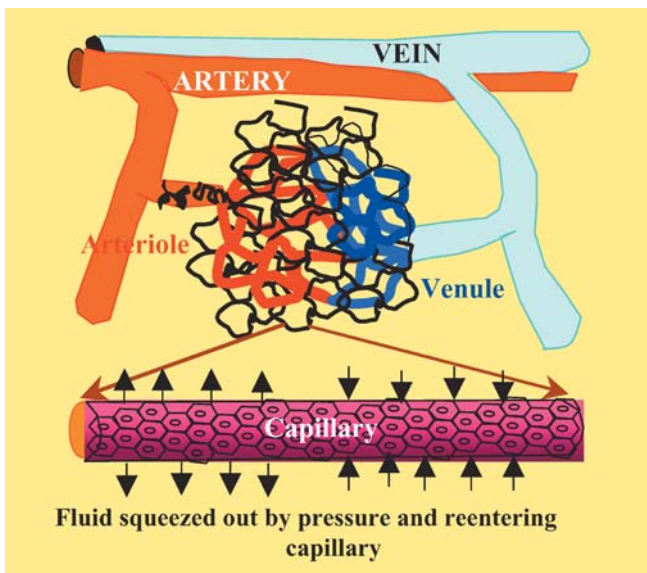


Fig. 7 Conceptual picture of the capillary bed and branching network of capillaries

as well as the passage of white blood cells. Nutrients, wastes and hormones are exchanged across the thin walls of capillaries. A schematic view of a capillary bed system is shown in Fig. 7.

In our model, the capillaries represent the boundary conditions and physical constraints for the blood flow. Compared to the continuum approach, the particle methods have serious technical difficulties with the definition of the complex boundaries for open systems because:

1. The particle system is closed.
2. It is impossible to define the boundaries for an “infinite” system, which can be only modeled using periodic boundary conditions.
3. The number of particles in the model without reactions must remain constant. Therefore, the number of particles leaving the system must enter it from the other side.

By using periodic boundary conditions we must take into account the correlations between inlet and outlet streams. Correlations decrease with a larger system. Capillaries scale linearly with the number of particles. These artifacts can be partially compensated by introducing a “thermalization zone”. This zone, however, introduces its own autocorrelations.

Up to now, only a few methods have been considered in the treatment of boundary conditions in a particle system under shear flow. [36] The popular method is to “freeze” some portions of the fluid described by particles and treat them as rigid bodies. We have used this method here. However, the particles are “frozen” only along the flow direction and can move along both the coronal and the sagittal directions. We can now model the quasielastic nature of the capillary wall. The axial elasticity is less important and can be neglected. This model is considered to be physically correct because in the real blood vessel the wall consists of a layer of endothelial cells. [12, 13] These cells cannot move, but can deform. They respond to the shear flow due to the blood. The wall particles interact with one another with forces similar to solid particles in the RBC cells. In contrast to RBCs, the wall particles have a nonzero Brownian force in order to avoid excessive energy dissipation and to model random deformation of the wall particles. In Fig. 8 we show the four models of arteries used.

Plasma suspension

Plasma has generally been assumed to have a Newtonian rheology. [1] However, plasma is essentially a polymeric solution, and for this reason, a number of experiments have been performed to investigate its viscoelastic or nonNewtonian nature. [37, 38]

In our model, the plasma together with the other blood components is regarded as a colloidal suspension. From the standpoint of fluid dynamics, a general problem in describing such fluids is the lack of adequate rheological models. For complex fluids, it is necessary to base the modeling approach on a microscopic description of the system, thus working from the smallest scales upward. Molecular dynamics is the most accurate and fundamental method [39, 40, 41] but it is too computationally demanding for most 3-D complex fluids problems because it would entail at least tens of millions of fluid particles.

Flekkoy et al. [42] have shown that the mesoscopic fluid-particle model can be derived from molecular dynamics by means of a systematic coarse-graining procedure based on a 3-D Voronoi quantization scheme. [43]

Fig. 8 Different capillary models

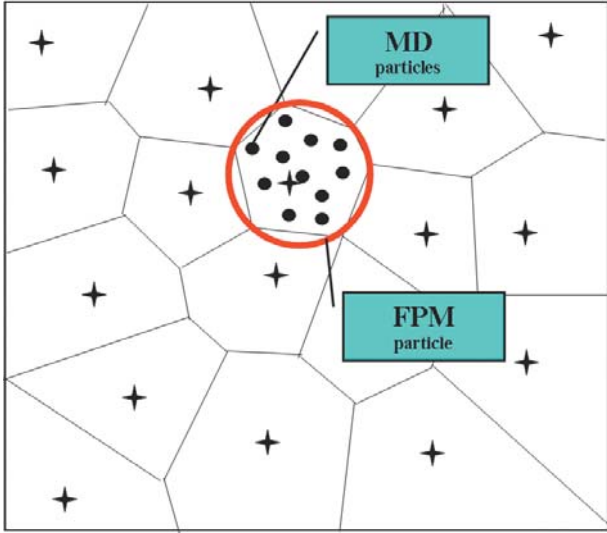
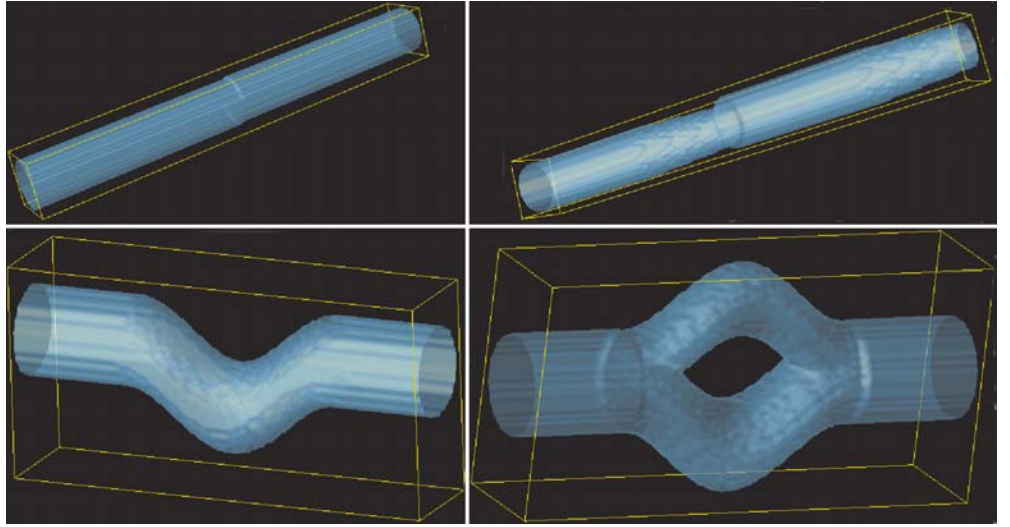


Fig. 9 The Voronoi tessellation in 2-D, and fluid particle made of MD particles

In Fig. 9 we exemplify the 2-D Voronoi tessellation. This procedure links the forces between the fluid particles to a hydrodynamic description of the underlying molecular dynamics (MD) particles. The fluid particles defined as cells on a Voronoi lattice with variable masses and sizes can be simplified to the form of dissipative particles of the fixed size and mass. These particles represent the basic entities of the DPD method [44] widely used for simulating colloidal mixtures in the mesoscale. [22, 23, 24, 25, 26, 27, 28, 29, 45] DPD can be understood as a *coarse graining* of the underlying molecular dynamics.

The most attractive features of the DPD technique lie in its versatility in providing simple dynamical models for complex fluids (see e.g. [26, 27, 28, 29, 45]). In DPD, the Newtonian fluid is rendered “complex” by defining additional forces between the fluid particles or by introducing an additional type of “solid” particles, i.e., particles interacting with a hard-core repulsive potential.

By changing just the nature of the conservative interactions between the fluid particles, one can easily construct polymers, colloids, amphiphiles and mixtures. [29, 45]

The fluid-particle model (FPM) [21] describing the plasma fluid differs significantly from the DPD model [44, 46] and also conventional MD. The fluid particles can rotate in space due to noncentral dissipative forces, which are lacking in DPD. The FPM particles should be understood as acting like relatively massive packets, although they are still particles in a statistical mechanical sense. The interactions between the particles are represented by the collision operator, with a finite range defined by Eq. (1). In contrast to the classical DPD, the interaction range for the fluid-particle model can be shorter due to the more realistic interaction potential between droplets in FPM. It reduces some of the deficiencies in the DPD model, [21, 46] which are usually compensated by a larger cut-off radius in the DPD interactions.

The “droplets” i and j of masses m_i , m_j and positions \mathbf{r}_i , \mathbf{r}_j interact with each other via a collision operator Ψ_{ij} . This type of interaction is a sum of the conservative force \mathbf{F}^C , two dissipative, noncentral components \mathbf{F}^T and \mathbf{F}^R (translational and rotational) and a Brownian force \mathbf{F} . The conservative forces cause the fluid particles to be evenly distributed in space by producing a certain “pressure” among them. The friction forces represent the viscous resistance between the various parts of the fluid, while the stochastic forces represent those degrees of freedom that have been eliminated during the coarse-graining process.

The collision operator, which is the sum of vector forces \mathbf{F}^C , \mathbf{F}^T and \mathbf{F}^R , can be written as:

$$\begin{aligned} \Psi_{ij} = & \{-\pi \cdot V'(r_{ij}) \cdot \mathbf{e}_{ij} - \gamma \cdot m(A(r_{ij}) \mathbf{1} + B(r_{ij}) \mathbf{e}_{ij}) \\ & \circ \left(\mathbf{v}_i + \left(\frac{1}{2} \mathbf{r}_{ij} \times (\tilde{\omega}_i + \tilde{\omega}_j) \right) \right) \mathbf{e}_{ij} + \sigma \left(A'(r_{ij}) d\tilde{\mathbf{W}}_{ij}^S \right. \\ & \left. + B'(r_{ij}) \frac{1}{D} \text{tr}[d\mathbf{W}] \mathbf{1} + C'(r_{ij}) d\tilde{\mathbf{W}}_{ij}^A \right) \circ \mathbf{e}_{ij} \} \\ & \cdot [\theta(\mathbf{r}_{ij}) - \theta(\mathbf{r}_{ij} - R_{\text{cut}})] \end{aligned} \quad (11)$$

where: $\mathbf{r}_{ij}=\mathbf{r}_i-\mathbf{r}_j$ is a vector pointing from particle i to particle j and $\mathbf{e}_{ij}=\mathbf{r}_{ij}/r_{ij}$, D is the model dimension, dt is the time step, γ is a scaling factor for dissipation forces, $\boldsymbol{\omega}$ is the angular velocity, $d\mathbf{W}^S$, $d\mathbf{W}^A$, $\text{tr}[d\mathbf{W}]\mathbf{1}$ are respectively the symmetric, antisymmetric and trace diagonal of the random matrices of the independent Wiener integral increments [21, 47] and $A(r)$, $B(r)$, $C(r)$, $A'(r)$, $B'(r)$, $V'(r)$ are normalized weight functions dependent on the separation distance r_{ij} .

The single-component FPM system yields the Gibbs distribution as the steady-state solution to the Fokker-Planck equation. Consequently, it obeys the fluctuation dissipation theorem, which specifies the relationship between the normalized weight functions, from which we can obtain the detailed balance condition:

$$T_0 = \frac{\sigma^2 m}{2k_B \gamma} \quad (12)$$

From the parameters associated with the fluid dynamical interactions of FPM, the fluid transport coefficients can be derived from kinetic theory in the continuum limit, [21, 46] as:

$$P = \frac{n \cdot \pi B_1}{2} \quad (13)$$

$$v_{\text{Bulk}} = \gamma \cdot n \left[\frac{A_2}{2D} + \frac{(D+2)}{2D} B_2 \right] + c^2 \frac{1}{\gamma n D [A_0 + B_0]} \quad (14)$$

$$\eta = \frac{1}{2} \gamma \cdot n \left[\frac{A_2}{2} + B_2 \right] + c^2 \frac{1}{\gamma n [A_0 + B_0]}$$

$$A_0 = \int A(r) d\vec{r}, B_0 = \frac{1}{D} \int B(r) d\vec{r}, B_1 = \frac{1}{D} \int r \cdot B(r) d\vec{r},$$

$$B_2 = \frac{1}{D(D+2)} \int r^2 \cdot B(r) d\vec{r}, A_2 = \frac{1}{D} \int r^2 A(r) d\vec{r} \quad (15)$$

where P is the partial pressure of fluid-particle ensemble, n the number density, T_0 the temperature of the particle system, η , v_{Bulk} shear and bulk kinematic viscosities, respectively, $D=3$, $c^2=k_B T_0/m$, and π , σ and γ scaling factors of conservative, Brownian and dissipative forces, respectively. In DPD [48] for a given T_0 , the viscosity is defined as a dimensionless quantity:

$$\Omega = \frac{\gamma \cdot R_{\text{cut}}}{3 \cdot v_T} \quad (16)$$

that represents a ratio between the thermal fluctuations and friction. Equations (14, 15, 16) were derived in the continuum limit for vanishing pressure, i.e., negligibly small value of the conservative force. In this fluid, the speed of sound is very low and the fluid becomes extremely compressible. One problem with the FPM, and also DPD, is that the conservative forces encourage a certain fluid behavior. The equation of state for the pressure, for example, was an outcome of the simulation and not an input. [21]

As shown in [27, 28, 29, 30, 31, 32, 33, 34, 35, 36, 37, 38, 39, 40, 41, 42, 43, 44, 45, 46, 47, 48, 49] for simulating realistic dynamics of complex fluids out of equilibrium, the pressure term should be large enough to en-

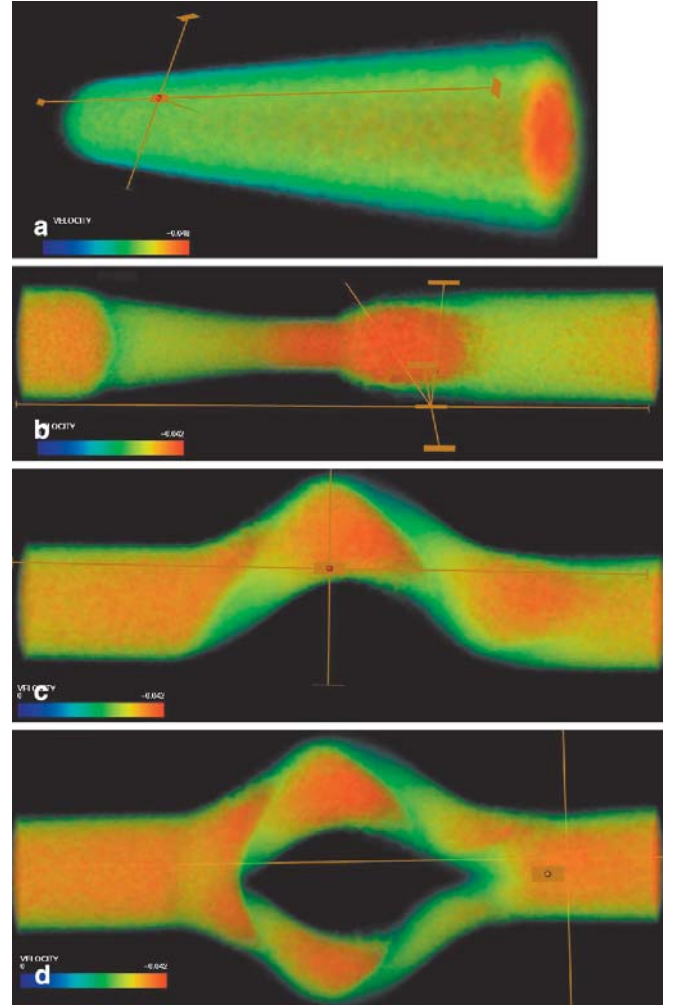


Fig. 10 The flow of fluid particles through the various shapes of vessels: (a) straight, (b) curved, (c) with choking point, and (d) with bifurcating capillaries. We show the scalar velocity field for V_z vector component. The influence of periodic boundary conditions can be observed from b. The flow starts from the left side. Dimensionless viscosity $\Omega=90$

sure prompt feedback between flow and microstructures formed by the colloidal beds. However, in [46] the transport coefficients computed from Eqs. (14, 15, 16) are underestimated because of the nonnegligible pressure term. The other alternative is to match the fluid viscosity a posteriori by solving the equations.

We have assumed that the plasma density and viscosity are similar to the density and viscosity of pure water. The initial viscosity can be defined a priori from Eqs. (14, 15, 16). Its actual value must be matched iteratively by using velocity profiles for the laminar Poiseuille flow.

We have investigated the flow dynamics in a long cylinder shown in Fig. 10a numerically. For a fully developed flow, the velocity profile is parabolic with an axial velocity distribution along the x coordinate $V_z(x)$:

$$V_z(x) = \frac{1}{2\eta\rho} \cdot \Delta p \cdot \frac{[(d/2)^2 - x^2]}{l_z} \quad (17)$$

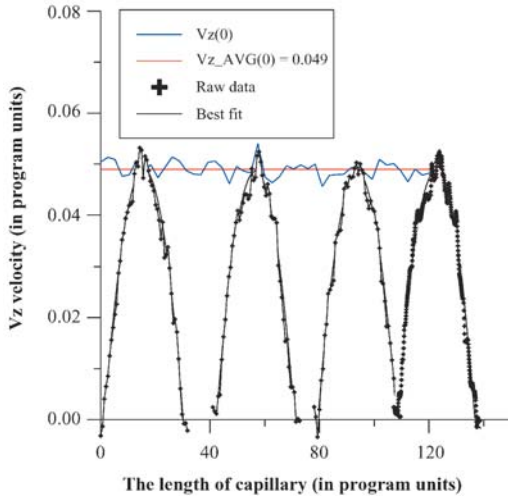


Fig. 11 Axial velocity of fluid particles along the capillary, and velocity profiles in selected sites of the capillary approximated by a second order polynomial

where Δp is the difference in pressure, d is the diameter of the capillary, l_z is the length of the capillary, and ρ is the density of the fluid. Therefore, from the velocity profiles shown in Fig. 11 we can easily estimate the viscosity value. We do not observe any distinct steady velocity profiles for the fluid particle models with negligible conservation force.

In Fig. 10 we display the axial velocity distribution V_z of the particle fluid flowing in four types of capillaries in the presence of periodic boundary conditions. From Fig. 10c,d we can recognize the areas of slower flow where the RBCs can be potentially trapped. Introduction of a “thermalization zone” in the outlet of the channels in Fig. 10b,c,d has not greatly improved the results. We have decided to use the pure periodic boundary conditions as a simplification.

RBC–fluid–wall interactions

The nonNewtonian characteristics of blood come from the cumulative interactions of RBC–RBC, RBC–plasma and RBCs–capillary walls. We have assumed that there are no attractive forces between blood cells, i.e., the particles from different cells (and the channel wall) rebound due to conservative repulsive forces modeled by the repulsive part of the Lennard-Jones force. The presence of particular plasma proteins, notably fibrinogen and immunoglobulins, plays an important role in the aggregation of blood cells. Many laboratory studies on blood flow suffer from the inability to eliminate thrombin, which activates the platelets, as well as preventing fibrin formation, which stabilizes platelet deposits. [1] Neglecting these factors allows us to examine other elements responsible for aggregation, which are directly associated with the capillary flow, such as RBC elasticity, viscosity and hydrodynamical forces. The particles forming RBCs

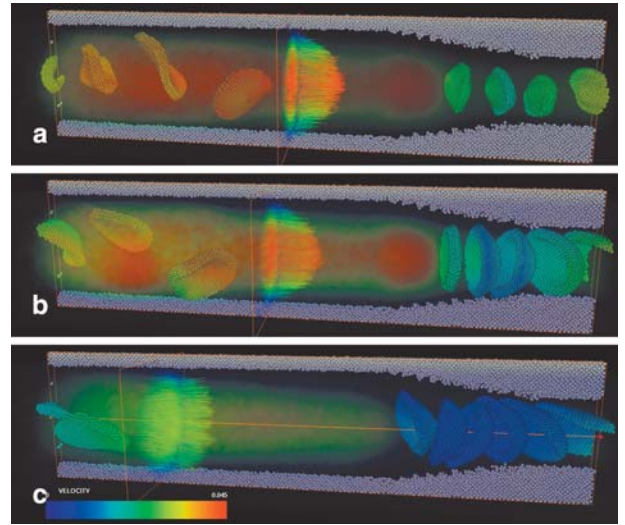


Fig. 12 RBCs flowing past the choking point for different viscosity of plasma suspension and the elasticity of blood cells. In (a), (b) and (c) we present the magnitude of the velocity fields and the cross-sections through the vector velocity fields for the same moment of time for the following plasma viscosity Ω and RBC elasticity π : (a) $\Omega=18$, $\pi=1$; (b) $\Omega=18$, $\pi=5$; (c) $\Omega=90$, $\pi=5$ (in program units). Periodic boundary conditions are employed

interact with the rest of the fluid with the same forces as the fluid particles (see Eq. 11), while the particles on the fluid–wall and RBC–wall interfaces interact only by means of repulsive forces.

The interactions of the blood cells with the walls and with the blood flow are responsible for RBC clustering. In order to illustrate the effects of these interactions, we have modeled RBCs flowing through a choking point of a periodic pipe. The snapshots from the simulation are shown in Figs. 12a–c and 13a–c. The simulation starts with the most convenient situation for clotting, i.e., all RBCs were placed in the perpendicular direction to the flow. In Fig. 12, in contrast to the situation from Fig. 11b, the velocity field close to the strangulation has the lowest magnitude because of blockage by the blood cells. However, the elastic discs are able to pass through because of the positive feedback between disc elasticity and the hydrodynamic forces accompanied by the interactions between RBCs and the wall. The flow for the plasma is laminar in this low Reynolds number ($Re \approx 1$) flow. As the streamlines in Fig. 13 reveal, this laminar situation dominates in the regions where there are no RBCs. The noise observed arises from the thermal fluctuations in the particle ensemble and from separate particles that percolate through the wall. The micro-viscoelastic properties of the particle system can be observed in Fig. 13, which shows the angular momentum distribution. The absolute value of the local angular momentum is distinctly higher close to the blood cells that leave the constriction point. This increase of local angular momentum can be regarded as micro-vortices. These vortices cannot be discerned clearly in velocity streamlines due to the low resolution of the velocity field and due to the

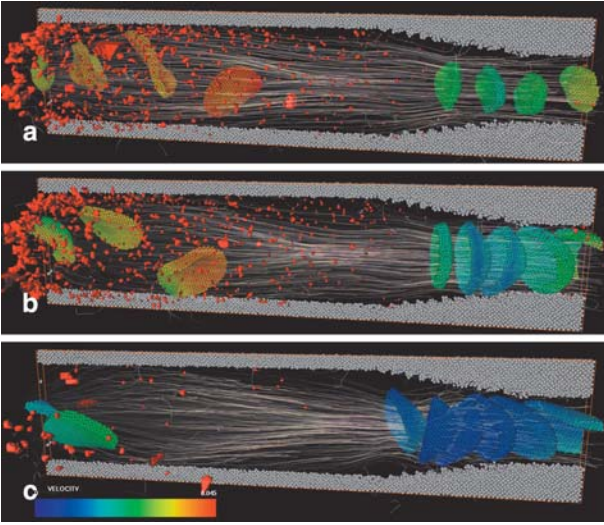


Fig. 13 RBCs flowing through the choking point for different viscosity of plasma suspension and the elasticity of blood cells. In (a), (b) and (c) we present the streamlines of blood flow for the same moment of time for the following plasma viscosity Ω and RBC elasticity π : (a) $\Omega=18$, $\pi=1$; (b) $\Omega=18$, $\pi=5$; (c) $\Omega=90$, $\pi=5$ (in program units). Red spots show the highest values of local angular momenta in the particle fluid. Periodic boundary conditions are applied. See the supplementary material with movie 13A

thermal fluctuations. In Fig. 13, we see that the local angular momentum is much greater for the particle fluid with smaller viscosity. These nonlinear perturbations in creeping flows with low Reynolds numbers were observed in laboratory experiments with micro-flows in a viscoelastic medium. [50]

Implementation details

Here we study an isothermal three-dimensional system, which consists of M particles confined in a long cylinder with periodic boundary conditions in the axial direction. The flow is directed from the left to the right. The particle system is accelerated by an external force, corresponding to a given pressure gradient. Discrete-particle models with several million particles are today still computationally demanding. The efficiency of their implementation is decided by three factors:

1. A fast and accurate scheme for time-integrating the equations of motion (Eqs. 1, 2, 3, 4, 5).
2. An algorithm for searching the neighboring particles.
3. Efficient parallelization of the code.

Equations of motion: time stepping in the numerical integration

It is necessary to integrate at least 10^5 time steps to obtain accurate blood flow statistics and dynamics in a long capillary. The value of γ – the scaling factor of dissipative forces $\mathbf{F}^{\text{T,R}}$ (see Eq. 11) – in the physical scales of

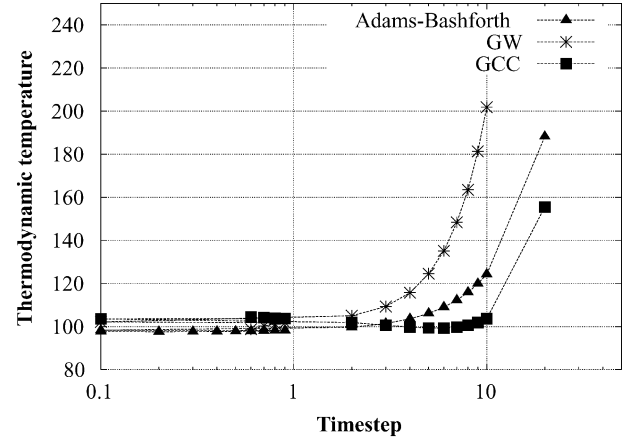


Fig. 14 Comparison of accuracy of the explicit Adams–Bashforth scheme and the predictor–corrector GCC [52] and GW [23] schemes

RBC should be large enough to match the realistic viscosity of the plasma. The viscosity represented by γ is coupled by the detailed balance equation (Eq. 12) to the Brownian force. The magnitude of the Brownian force depends on the time step Δt . For large values of γ and Δt , the dissipative force may appear to be greater than the Brownian force. Therefore, the value for Δt value should be small to obtain correct values of the transport coefficients. This difficulty becomes even more acute in modeling dynamical situations such as fluid dynamical mixing. Large velocity gradients increase the numerical error, causing a smaller Δt . Therefore, we need a stable, fast and accurate scheme for integrating the equations of motion in time.

The equations of motion (Eqs. 1, 2, 3, 4, 5) represent stochastic differential equations (SDE) due to the stochastic nature of the Brownian force. Therefore, the classical numerical schemes are only a crude approximation of the stochastic integrator. The *leap-frog* numerical scheme as in [51] is not suitable for integration of the equations of motion because the scheme is unstable for the FPM collision operator, which depends on both translational and angular velocities. The predictor–corrector schemes for integrating DPD equations [23, 52] consume twice as much computational time for evaluating the interparticle forces than explicit schemes such as the Verlet scheme. In FPM, unlike in DPD, the collision operator depends not only on the translational but also on the angular velocities, which additionally make the schemes more complex. Therefore, we have decided to use an explicit, higher-order time-stepping $O(\Delta t^4)$ scheme for ω : [28]

$$\omega_i^{n+1/2} = 2\omega_i^{n-1/2} - \omega_i^{n-2/3} + (N_i^n - N_i^{n-1}) \quad (18)$$

while the values of \mathbf{v}^{n+1} and ω^{n+1} are predicted by using a $O(\Delta t^2)$ Adams–Bashforth method. As shown in [28], both the hydrodynamic temperature and hydrodynamic pressures do not exhibit a noticeable drift after 1 million time steps in 2-D. In Fig. 14, we compare the accuracies for the three schemes, obtained from simulation of fluid

particles flowing in a long cylinder. It shows that the explicit scheme falls between GW and GCC predictor–corrector schemes, which are twice as time-consuming computationally. For simulations requiring more accurate conservation of thermodynamic quantities, a scheme with a thermostat [53] should be employed.

The algorithm for evaluation of various forces

Calculating the forces among FPM particles is very difficult due to the variable list of the particle neighbors. The particles interact with short-ranged forces defined by Eq. 1. For a multi-component system of fluid and solid particles with different interaction ranges, we have assumed that the cut-off radius $R_{\text{cut}} \sim \max_k (R_{\text{cut}, k})$. The particular value of k indicates the type of interaction. We have used the same R_{cut} for all the interactions except for those between wall particle–wall particle and RBC particle–RBC particle (for the same cell), which use invariable neighbor lists. The forces in an FPM fluid are computed by using an $O(M)$ order *link-list* scheme. [39] The force on a given particle includes the contributions from both solid and fluid particles closer than R_{cut} and those located within the cell containing the given particle or within the adjacent cell. A system of 10 million fluid particles requires the evaluation of 10^{10} floating point operations at each time step.

Computational implementation

Parallel computing is very efficient for speeding up large-scale calculations, but requires a hard job of decomposing the computation into processes and mapping them onto the multiple processors. The total volume of the box is divided into P overlapping subsystems of equal volume, and each subsystem is assigned to a single processor in a P -processor array. By using the SPMD paradigm (*single program multiple data*) commonly used for MD code parallelization, each processor follows an identical predetermined sequence to calculate the forces on the particles within its assigned domain. The implementation details and the FPM parallel code are provided in [54].

For this blood model we have made the following modifications in the FPM code:

1. The RBC particles have an invariable neighbor list, which is computed only once at the beginning.
2. The particles from RBCs are identified by particular identification numbers, because two particles from two different RBCs interact in a different way from similar particles situated inside a single RBC. This particle index is a combination of the particle number, RBC number and the process number.
3. The index array has a global data structure accessible by each processor.
4. To speed up the search in this global array, we have defined additional local arrays associated with each

process. These arrays contain the indices to the RBC particles simulated exclusively by a specified process.

5. A load-balancing procedure was added for ensuring the same computational load for each processor. The load cannot be uniform, as it is for a pure FPM code, [54] due to the inhomogeneous distribution of clots generated, e.g., by the pressure of the choking point.

The code was written in FORTRAN 95 and was implemented on the MPI interface for the IBM SP with WinterHawk+nodes consisting of 4 Power3+/375 MHz processors with 8 GB of RAM memory per node, SGI/Origin 3800 with two R14000/500 processors with 8 GB of memory and Sunblade 2000 workstations with two UltraSparc III/900 processors sharing 6 GB of memory. The average computational time for the runs presented in Figs. 12 and 13 involving about 1 million particles in 3×10^3 time steps is approximately 5–8 wall clock hours on four SGI/Origin 3800 R14000/500 processors. For runs with 1 million particles we have used four processors, while for the runs with 10 million we used from 16 to 32 parallel processors. We visualize all of the data by using the recent visualization package Amira 2.3 (<http://www.amiravis.com>, [55]) on an SGI/Origin 3800.

Results

Principal parameters of the discrete particle system

The principal parameters of this particle system are summarized in Table 1. They are given in both program units and physical units matched to two different models of simulation: a large RBC model and a small RBC model, representing different physical scales. The first scale was matched to the situation shown in Figs. 12 and 13, where the diameter of the capillary is on the same order as the RBC diameter. In modeling flow along larger capillaries with a greater number of blood cells, we have defined the diameters of RBCs three times smaller than before for the same number of particles. In both cases we obtain the physical unit of length by rescaling the RBC diameters, given in program units, to the maximal actual size of RBC cell, i.e., $10 \mu\text{m}$. We have matched the rest of the physical units by using this unit length and the thermalized velocity v_T .

As shown in Table 1 and in [23, 49] the matching of spatio-temporal scales of the DPD and FPM models to the actual physical units poses a serious problem due to the unclear physical spatio-temporal scales captured by the numerical method. Realistic units of length and time in the fluid particle model are defined by the average distance between particles λ and the fluctuations generated by the Brownian component represented by the thermal velocity $v_T = \sqrt{kT/m}$. It appears that at scales of the order of a red blood cell, the value of v_T is approximately equal to the blood velocity in the vessels, i.e., millimeters per second. Simulation of this type of creeping flow by using particles is still very demanding. Table 1 shows

Table 1 The principal parameters of the particle system

| Unit name | Definition | Values in program units | Physical parameters for large cells model | Physical parameters for small cells model |
|---------------------------------|--|------------------------------|---|--|
| RBC size | Largest diameter of RBC cell | | 20 (in program units) 10 μm | 6.3 (in program units) 10 μm |
| Unit of length | Hockney cell size | 1 | 0.5 μm | 1.58 μm |
| Cut-off radius R_{cut} | $R_{\text{cut}}=L\lambda$, we have used $L=1.6$ | 0.99 | 0.5 μm | 1.57 μm |
| Particle spacing λ | $\lambda=1/n^{1/3}$ | 0.63 | 0.31 μm | 1.0 μm |
| Number density n | Number of particles per cell | 4 | 3.2×10^{19} part m^{-3} $\rho=1030$ kg m^{-3} | 10^{12} part m^{-3} $\rho=1030$ kg m^{-3} |
| Unit of mass | Fluid particle mass m_1 | 1 | 3.13×10^{-17} kg | 1.03×10^{-15} kg |
| | Mass of the RBC particle m_2 | 1.14 | 3.55×10^{-17} kg | 1.17×10^{-15} kg |
| Unit of time | Δt -time step size | 1 | 1.61×10^{-7} s | 3.01×10^{-6} s |
| Computer time | Number of time steps for a single run | 3,000 | 4.92×10^{-4} s | 9.03×10^{-3} s |
| Temperature | T_0 | | 310 K | 310 K |
| Thermalized velocity | $v_T=\sqrt{(kT/m_1)}$ | 0.0036 | 0.0110 m s^{-1} | 0.0019 m s^{-1} |
| Characteristic time | λ/v_T | 175 | 2.81×10^{-5} s | 5.26×10^{-4} s |
| γ (see Eq. 11) | Scaling factor of dissipative forces (see Eqs. 14, 15, 16) | 1.5–7.5 | $9.1\text{--}45.5 \times 10^6$ s^{-1} | $5.0\text{--}25 \times 10^5$ s^{-1} |
| Ω (see Eq. 16) | Ratio between the friction and thermal fluctuations | 18–90 | 18–90 | 18–90 |
| Kinematic viscosity | Kinematic viscosity computed a posteriori for $\Omega=90$ | Plasma 0.51 Blood 0.9–1.2 | 0.79×10^{-6} m s^{-2} – | 0.42×10^{-6} m s^{-2} – |
| P (see Eq. 11) | Scaling factor π is proportional to P (see Eqs. 13). The first value is for FPM, the second stands for the elasticity of RBC particles | 0.00082, 0.11 | 1.9 Pa, 245 Pa | 0.06 Pa 7.29 Pa |
| l_z (see Eq. 17) | Length of the capillary | 128–256 | 64–128 μm | 202–404 μm |
| d (see Eq. 17) | Diameter of the capillary | 26 | 13 μm | 41 μm |
| v_{max} | Maximum velocity of the blood flow | 0.05 | 0.13 m s^{-2} | 0.022 m s^{-2} |
| Re | Reynolds number for pure blood plasma | 3.8 | 3.8 | 3.8 |
| Shear rate | $\Gamma=v_{\text{avg}}/d$ | 10^{-3} | 5.0×10^3 s^{-1} | 2.68×10^2 s^{-1} |
| Number of particles | Particles in total – 1.05×10^6 FPM particles – 5.04×10^5 | RBC particles – | 5.2×10^4 | |

that the blood velocity assumed in our model for large RBC is much higher, about 13 cm s^{-1} . However, it persists for a relatively short time, i.e., 0.5 ms. Flow in a blood capillary is unrealistic under normal conditions but very feasible in extreme situations, such as crisis moments involving stroke and large accelerations in jets or car accidents.

The numerical problem with high speed blood can be compensated partially by assuming a larger physical scale of the model, thus decreasing the influence of thermal fluctuations. This situation corresponds to the model with small RBCs, for which the blood velocity has a reasonable value. The plasma viscosity is now about six times smaller than the actual physical value. As in the previous model, higher viscosity can be obtained by decreasing the time step about one hundred times. For the size of time step used and for the large value of γ corresponding to a high viscosity, the Brownian force cannot keep pace with the dissipative forces. Eventually, the program halts due to numerical blow up.

A low viscosity model is useful for studying the rheological properties of whole blood. Blood viscosity is about 5–10 times higher than that for the plasma suspension and it is interesting to determine the extent to which

the plasma viscosity influences the blood viscosity. The viscosity of plasma can be decreased easily to a low level by the presence of blood thinners or alcohol.

In the following models, we have assumed a low hematocrit, which is about 11% for small RBC and 7% for large RBC models. This is the lower acceptable value for the blood flowing in small capillaries. We have used 1.1 million particles in these calculations. A comparison of the wall clock times between MD and FPM shows that the FPM requires approximately the same computational time as the classical short-ranged MD but for 10 million particles.

A fluid with initial velocity 0.05, in program units, is accelerated by the pressure difference Δp (Eq. 17) to the steady-state laminar flow. Initially, the RBCs are perpendicular to the blood flow. In the next section we present the results obtained both for the small and large RBC models in different types of flows.

Straight capillary

We present the results from blood flowing in a straight capillary. The pipe inlet and outlet are somewhat (<5%)

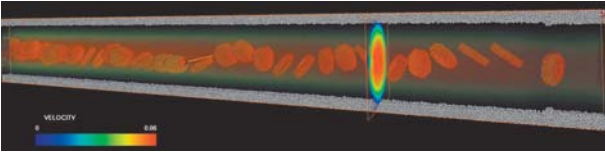


Fig. 15 RBCs flowing in a straight capillary. We display the velocity field. The *red* color represents the highest velocity. The image shows the situation after stabilization of the flow (3,000 time steps – 0.5 ms). The pressure difference Δp (Eq. 17) is three times greater than that for a similar model with a pure plasma (Fig. 10a)

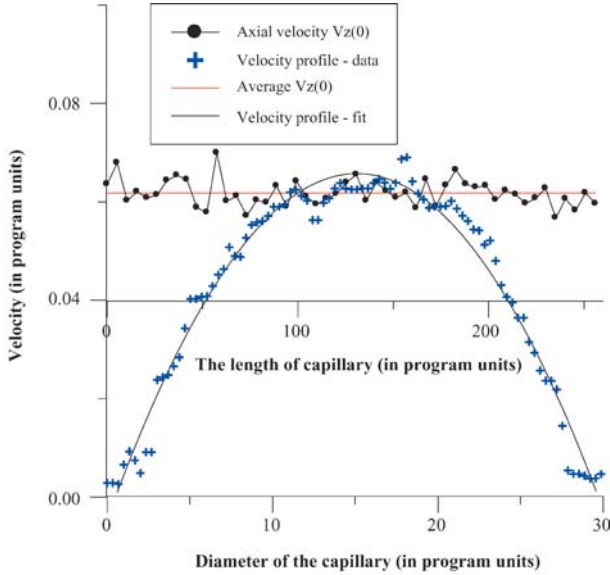


Fig. 16 Axial velocity along the capillary from the velocity field displayed in Fig. 15. The velocity profile from the cross-section shown in Fig. 15 is approximated by a quadratic function

choked to perturb the flow of RBC cells. In Fig. 15 we show the snapshot from the large RBC model for the viscosity of the plasma $\eta=0.79 \times 10^{-6} \text{ m s}^{-2}$. This value is 20–30% lower than the realistic viscosity for the plasma suspension. The flow is laminar and we do not observe any clustering of the blood cells.

From the data shown in Fig. 16 and from Eq. (17), we can estimate the viscosity of the system, which is 2.37 times greater than that for the pure plasma suspension. For a similar shear rate, the kinematic viscosity for blood in larger arteries is about $\eta=2\text{--}3 \times 10^{-6} \text{ m s}^{-2}$ assuming that the hematocrit is 40% (see <http://www.cheng.cam.ac.uk/~rmdr2/research.html>). We have used a hematocrit value of 7%.

The situation is different for a small RBC model, which represents a larger physical scale of the blood flow. The hematocrit is now 11% and is higher than for the large RBC model. We compare the results from the two runs with different viscosities of the plasma suspension. The viscosities can be matched approximately a priori by using Eqs. (14, 15) and the dimensionless value of Ω (Eq. 16). These values are corrected a posteriori based on

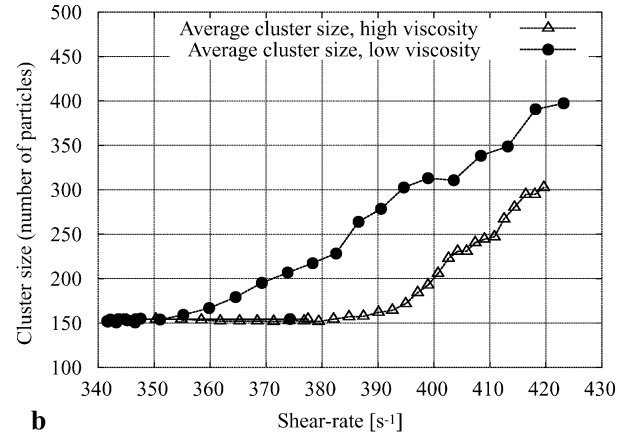
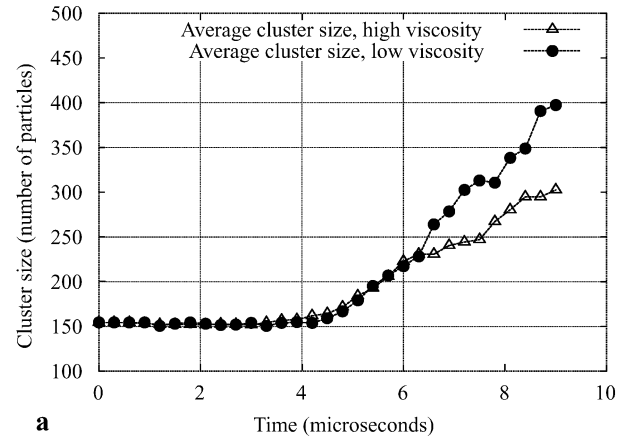


Fig. 17 The average cluster size (a) in time and (b) as a function of the shear rate for two flows with high and low viscosities

the velocity profiles and Eq. (17). We evaluate the average cluster size in time. We have extracted clusters by using the parallel clustering procedure described in [56].

In Fig. 17a,b one can observe that clustering of RBCs occurs initially as single clusters, each consisting of 150 particles. During the time interval of 6 μs , the growth in the average cluster size is identical for both high and low Ω . The only difference is in the shear rate, which is higher for the lower Ω case. An increase in the average cluster size is accelerated for shear rates greater than 400. As shown in Fig. 18a,c, this speed-up is caused by the sharp concentration of RBCs in the center of the capillary. The cluster growth in the high viscosity fluid is moderate and stabilizes at the end. In Fig. 18b,d we show that for high Ω the clusters are produced mainly close to the capillary walls. This is due to the high velocity gradient in the x - y cross-section, which adjusts much faster than for the higher viscosity fluid. In Fig. 19 we display the instant of the birth of a cluster close to the wall caused by different speeds of FPM particles from the central flow stream and those in the proximity of the capillary walls. A high-resolution picture from the simulation with 10 million particles can be found in the supplementary material.

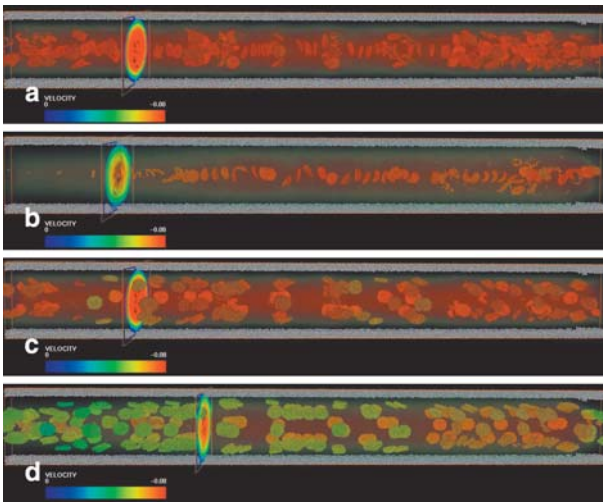


Fig. 18 RBCs flowing through a straight capillary for different values of Ω . In (a) and (c) $\Omega=18$ and in (b) and (d) $\Omega=90$. We display the velocity field and axial cross-section from the field. *Red* color represents the highest velocity. The first two images show the blood cells located close to the center of the flow. The next two show the cells close to the wall

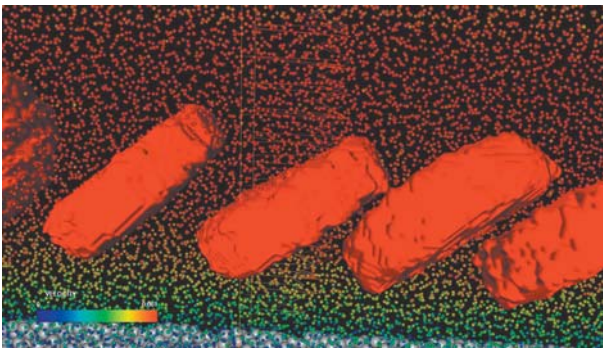


Fig. 19 Clustering of RBCs produced by velocity boundary layers close to the capillary walls. Only the thin slice throughout the FPM fluid is shown. The fastest particles are colored in *red*, the slowest in *blue*. See the supplementary material 19A with picture from a high-resolution model with 10 million particles

The kinematic viscosity of blood computed from the velocity profiles by assuming high Ω is only 80% greater than for the pure plasma suspension with the same value of Ω . It is also two times greater than for a low Ω fluid.

This result may suggest that for very viscous blood there are many RBC clusters close to the capillary walls. This situation accelerates thrombus production when a blood vessel is cut or injured. Consequently, in blood with a lower viscosity the clusters tend to remain mainly in the center of flow. In a more vigorous blood flow, the thrombus production close to the capillary wall will be more difficult for low viscosity blood.

The clustering of the blood cells at a choking point for the large RBC model was discussed in the section Numerical model. Similar behavior can be observed for the small RBC model. As we show in [57], these find-

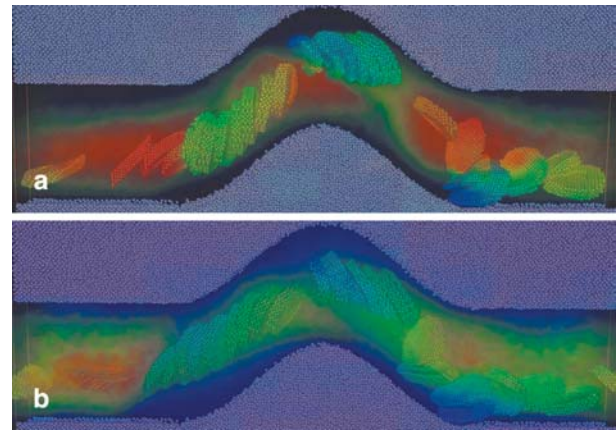


Fig. 20 Blood cells flowing along a long, curved capillary for two different viscosities: (a) $\Omega=18$, (b) $\Omega=90$. *Red* color corresponds to the highest velocity, which is approximately equal to 0.03 in program units

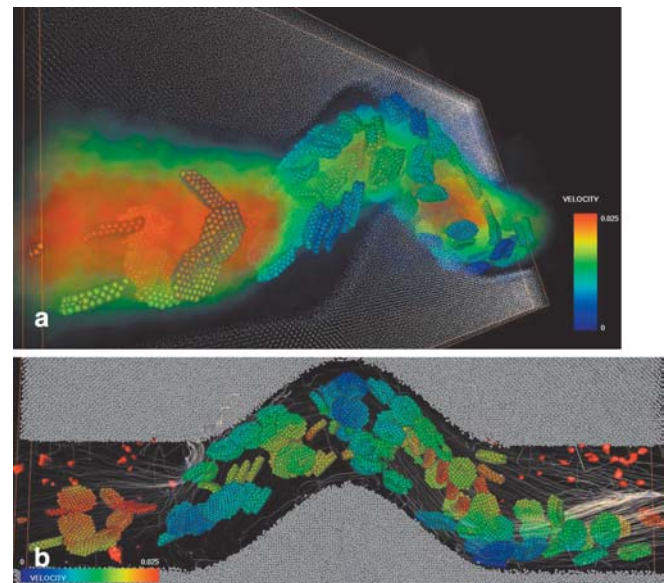


Fig. 21 Snapshots from a small RBC model for $\Omega=90$. In (a) we show the magnitude of the velocity field and in (b) the faint streaks of streamlines are depicted in *gray*. The *red* spots represent the highest local angular momentum developed in the plasma fluid

ings confirm the medical observations concerning clotting of distorted cells close to the choking point. The “sickle” blood cells are unable to squeeze through the smaller arterioles and capillaries. “Sickle”-shaped RBCs often adhere to the small blood vessels and halt the blood flow. In most cases, decreasing the blood viscosity prevents the clotting of RBCs at the choking points.

Curved and bifurcating capillaries

In Figs. 20a,b and 21a,b we show snapshots from simulations of blood flowing in curved capillaries for the large RBC model. In contrast to the straight capillary for

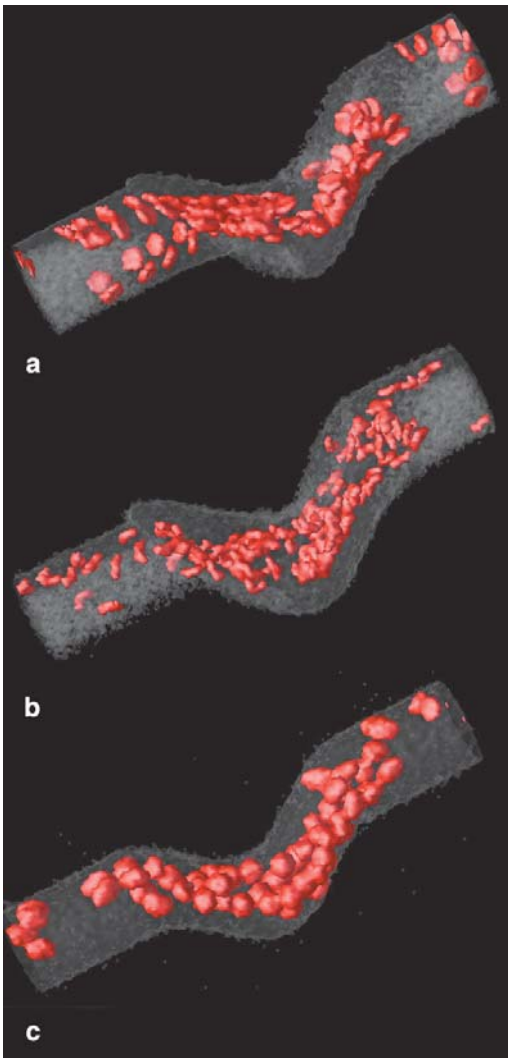


Fig. 22 The snapshots from RBCs flowing in a curved capillary vessel for (a) normal, biconcave blood cells, (b) “sickle”-shaped cells and (c) “spherical” cells. See the supplementary material with movies 22A,B,C. Rarefaction waves due to viscoelasticity can be observed in the movies

the large RBC case, we observe the formation of clusters in the inlet and inside the curved part of the channel. The clusters are spread out at the outlet. A similar behavior is revealed for both high and low velocities. The only differences are in the shear rate, which is higher for the low viscosity fluid. Higher stress makes the clusters more compact, which can be crucial for the clotting process. The rouleaux come partly from the initial conditions assumed. For the scales modeled, this type of initial structure is very likely (see the pictures from electron microscopy <http://kumc.edu/instruction/medicine/anatomy/histoweb/vascular/vascular.htm>).

In contrast to the large RBC model, the clusters produced by the small RBC model are more complicated, but still very clear. For the situation shown in Fig. 21 ($\Omega=90$), the largest clusters are located close to the capillary wall. Due to complicated interactions between flu-

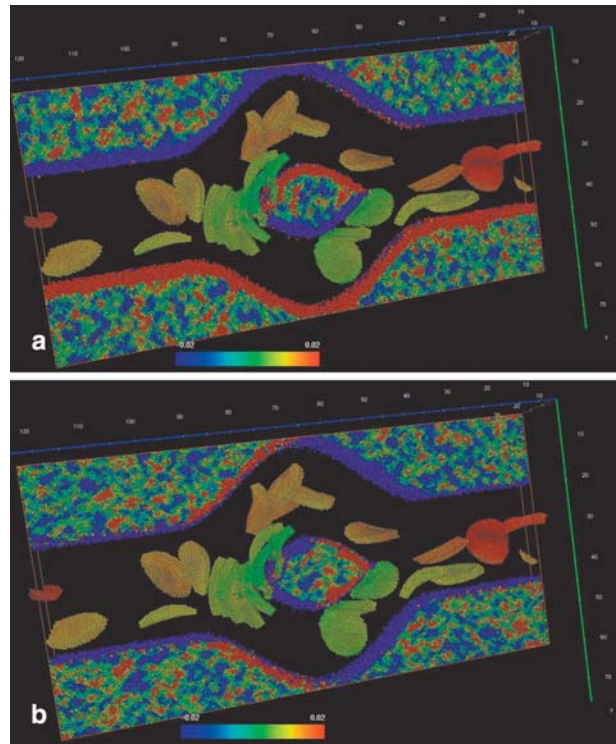


Fig. 23 Blood cells flowing through a bifurcating capillary ($\Omega=90$). We display how the wall reacts to the flow. *Red* and *violet* represent the maximal negative and positive velocities, respectively. **a** represents the V_y and **b** the V_z components of the velocity field. See the supplementary material 23A with movie

id-walls-RBCs, the flow is no longer laminar as in Fig. 18. The streamlines are not smooth and the particles have much larger spin than for the flow in the straight channel. The small rouleaux clusters and single cells create more loosely coupled structures in the curved fragment of the capillary. These situations are revealed more clearly in Fig. 22a–c.

We can see that there are not many differences between the large clusters created by the blood cells of various shapes. There are only small variations of flow patterns, which come from different weights and speeds of variously shaped RBCs. Light, “sickle” cells flow most smoothly along the axial line of the capillary. The normal cell rebound from the walls at places with the most stagnant plasma flow (see Fig. 10c), which is shown in Fig. 22a by the arrows. This behavior is even better illustrated for the large spherical cells (Fig. 22c).

The reaction of the wall to the blood flow can be observed for bifurcating capillaries. From the directions of velocity field components V_y and V_z for the wall particles, displayed in Fig. 23a,b, one can see that the hydrodynamic pressure tries to expand the capillary wall in the y and z directions. The pressure generates high stresses in the bifurcation zone. As shown in Fig. 23, additional stress in the bifurcation zone is produced by the clotting of blood cells. Under extremely high acceleration, this type of clotting can stop the flow altogether or disrupt

the capillary. A similar behavior is found for RBCs with various shapes and with a lower viscosity blood.

Unlike the capillaries, the stress in the bifurcation zone becomes very small for the oscillatory flow of blood in large arteries. [15, 58] This is a consequence of the difference in the nature of the macroscopic flow and the back reaction of the vessel wall back on the flow. The walls in the large arteries are elastic. In capillaries, the wall is made of a layer of endothelial cells, which cannot move but can deform elastically. In the high acceleration field the mechanical force exerted by the clotting cells can be enough to rupture very delicate junction points in the bifurcation zone. Wholesale bleeding from the capillaries suffered under extreme circumstances, such as high acceleration, mechanical shocks and internal strokes, can be as fatal as the blood diseases in macroscopic arteries.

Concluding remarks

A general deterministic approach for modeling blood is impossible because of the multiresolutional character of the vascular system with the individual components ranging from micrometers to tens of centimeters. Rapid progress is currently being achieved in blood flow studies in large arteries. Surprisingly, apart from a few simplified models, the dynamics and clustering of the RBCs in capillaries have been investigated only experimentally (see, e.g., [2, 59]).

The problems addressed here involve the challenges of modeling blood dynamics over scales four orders of magnitude smaller than those captured by classical fluid dynamics. On the basis of the DPM, we can follow the dynamics at this scale, which can reproduce realistic behavior of RBCs flowing in capillaries. This model is entirely mechanistic and stochastic. The discrete particles represent clusters of matter, which can be understood as a *coarse-graining* of molecules.

We have studied a three-component system consisting of RBCs, plasma suspension and capillaries. We may also incorporate other blood components, such as platelets and fibrin, artificial blood substitutes and simple chemical reactions. The nature of the conservative forces can be modified easily. Thus, it is possible to model the cross-scale process of cell–cell adhesion, which may arise from fibrinogen at varying concentrations.

The DPM allows a direct insight into fundamental processes, such as clotting. We have dealt with RBC clustering in capillaries of different shape. Despite the lack of attractive forces between the RBCs, they form clusters of various sizes depending on the type of flow and the values of the transport coefficients. This clustering mechanism, which is entirely reversible, can influence the process of RBC clotting both in geometrical “traps” such as choking points and curvatures of the capillaries and in the case of a cut or damage to the capillary walls. We show that blood rheology depends strongly on the viscosity of the plasma, which plays a very important

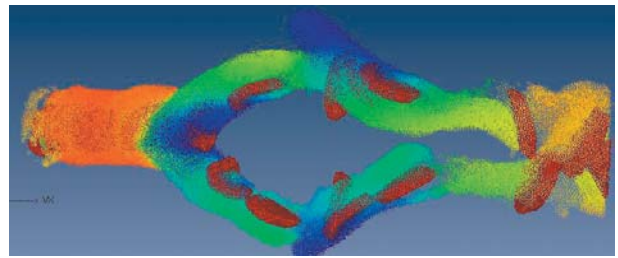


Fig. 24 Discontinuities in the plasma flow and free surface of the fluid simulated by using attractive force between the FPM particles. The RBCs are colored in *red*. The other particles have colors representing their respective velocity values. The *red* stands for the highest velocity and the *blue* for the lowest

role in clotting. Hydrodynamical forces in plasma with the higher viscosity are mainly responsible for clustering of the RBCs close to the capillary walls. Otherwise, for the plasma with the lower viscosity, RBCs can accumulate mainly in the central section of the flow.

Depletion forces are the natural outcome of the model because the fluid is made of particles. The forces must be greater in the small RBC model, for which the fluid-particles are greater than the fluid-particles in the large RBC model. Realistic values of depletion forces depend on how large the physical size of the FPM particle can be. Therefore, the influence of the excluded volume effect on clustering cannot be studied without constraints from the experimental results. The influence of depletion forces on clustering can be much smaller than hydrodynamic forces. In the future this problem should be studied more carefully.

Numerical studies of RBC flow for realistic velocities and transport coefficients by using this model is a challenging task due to computationally demanding processes of searching for the neighbors and computing the forces in a discrete-particle ensemble. Greater computational efficiency can be gained by making the following improvements.

1. More sophisticated time-stepping schemes (such as [53]) can be used, which allow for larger time steps.
2. One can employ a larger number of parallel processors.
3. We can define different conservative forces.

Taking into account the above and the ongoing increase of the processor speed, we will be able to model blood in normal conditions in the near future.

One can solve at least two problems by using conservative forces with an attractive tail. The viscosity of blood can be increased without increasing the time step and the modeling of surface tension becomes possible. In Fig. 24 we show an example of a simulation carried out assuming attractive forces between FPM particles. The discontinuities of the particle fluid can be observed easily. We are confronted with the problem of how to visualize these flow situations with discontinuities and how to control not only the viscosity but also the other thermo-

dynamic parameters of the particle system. For the model with the repulsive conservative forces, the viscosity can be controlled partially by the Ω value with all the other parameters such as pressure, temperature and density defined a priori. A particle system dominated by attractive conservative force behaves in a completely different way. In order to control a priori all the thermodynamic parameters, we must replace the FPM with a new thermodynamically consistent model of fluid particles such as that described in [60]. The computational implementation of this model can be difficult.

The mortality rate of people suffering from cardiovascular diseases is one of the highest. Therefore, a clear understanding of the biomechanical and biochemical processes taking place in the microscopic circulatory system is a very fundamental problem in the medical sciences. We believe that numerical modeling of these processes by using the discrete-particle approach will lead to important new insights in addressing these issues.

Supplementary material

Additional information about several figures is available in the supplementary material.

Acknowledgments We thank Drs Bill Gleason and Dan Kroll for very useful discussions. Support for this work has come from the Polish Committee for Scientific Research (KBN) project 4 T11F 02022, the Complex Fluid Program of U.S. Department of Energy and from AGH Institute of Computer Science internal funds.

References

- Fung YC (1993) *Biomechanics*. Springer, Berlin Heidelberg New York, p 515
- de Roeck RM, Mackley MR (1997) The rheology and microstructure of equine blood. www.cheng.cam.ac.uk/~rmdr2/research.html
- Diamond SL (2001) *Biophys J* 80:1031–1032
- Kuharsky A, Fogelson A (2001) *Biophys J* 80:1050–1074
- Hitt DL, Lowe ML (1996) Spatial analysis of red blood cell aggregation for in vitro tube flow. In: Proceedings of the 6th World Congress on Microcirculation. Munich, Germany
- <http://www.cardioliving.com/consumer/Circulatory/Clotting.shtm>
- Hitt DL (1999) Simulations of observed power spectra of aggregating blood flow under videomicroscopy. In: Goel VK (ed) Proceedings of the 1999 ASME Bioengineering Conference, BED-vol 42. American Society of Mechanical Engineers, New York, pp 543–544
- Shrinivasan S, Peach JP, Hitt DL, Eggleton CD (2001) Rheology of mixtures of artificial blood and erythrocyte suspensions. In: Proceedings of the 2001 ASME Bioengineering Conference. American Society of Mechanical Engineers, New York
- Hitt DL, Lowe ML (1997) Confocal imaging and numerical simulations of converging flows in artificial microvessels. In: Gourley P (ed) Proceedings of Micro- and Nanofabricated Electro-Optical Mechanical Systems for Biomedical and Environmental Applications, vol 2978. Society of Photo-Optical Instrumentation Engineers (SPIE), Bellingham, WA, pp 145–154
- Hitt DL, Lowe ML, Tincher JR, Watters JM (1996) *Microcirculation* 3:259–263
- Hitt DL, Lowe ML (1999) *ASME J Biomech Eng* 121:170–177.
- <http://gened.emc.maricopa.edu/bio/bio181/BIOBK/BioBookcircSYS.html#The%20Heart>, vol 2978
- <http://www.lab.anhb.uwa.edu.au/mb140/CorePages/Vascular/Vascular.htm>
- McDonnald DA (1974) *Blood flow in arteries*. Edward Arnold, London
- Botnar R, Rappitsch G, Scheidegger MB, Liepsch D, Perktold K, Boesiger PJ (2000) *Biomechanics* 33:137–144
- Acrivios A, Mauri R, Fan X (1993) *Int J Multiphase Flow* 19:797–802
- <http://kumc.edu/instruction/medicine/anatomy/histoweb/vascular/vascular.htm>, item: Capillary
- Wolfram S (2002) *A new kind of science*. Wolfram Media, p 1263
- Dzwiniel W, Alda W, Kitowski J, Yuen DA (2000) *Mol Simulat* 25:6361–6384
- Dzwiniel W (1997) *Future Gener Comput Sys* 12:1–19
- Espanol P (1998) *Phys Rev E* 57:2930–2948
- Coveney PV, Novik KE (1996) *Phys Rev E* 54:5134–5141
- Groot RD, Warren PB (1997) *J Chem Phys* 107:4423–4435
- Clar AT, Lal M, Ruddock JN, Warren PB (2000) *Langmuir* 16:6342–6350
- Omelyan I (1998) *Comput Phys* 12:97–103
- Dzwiniel W, Yuen DA (1999) *Mol Simulat* 22:369–395
- Dzwiniel W, Yuen DA (2001) *Int J Mod Phys C* 12:91–118
- Dzwiniel W, Yuen DA, Boryczko K (2002) *J Mol Model* 8:33–45
- Dzwiniel W, Yuen DA (2002) *J Colloid Interf Sci* 247:463–480
- Quarteroni A, Tuveri M, Veneziani A (2000) *Comput Vis Sci* 2:163–197
- Leuprecht A, Perktold K, Prosi M, Berk T, Trubel W, Schima H (2002) *J Biomech* 35:225–36
- Karner G, Perktold K (2000) *J Biomech* 33:709–15
- Lafaurie B, Nardone C, Scardovelli R, Zaleski S, Zanetti G (1994) *J Comput Phys* 113:134–47
- Lelièvre JC, Bucherer C, Geiger S, Lacombe C, Vereycken V (1995) *J Phys III France* 5:1689–1706
- Chopard B, Droz M (1998) *Cellular automata modeling of physical systems*. Cambridge University Press, Cambridge
- Revenga M, Zuniga I, Espanol P (1998) *Int J Mod Phys C* 9:1319–1328
- Kasser U, Heimburge P, Walitza G (1989) *Clin Hematology* 9:307–312
- Thurston GB (1996) Viscoelastic properties of blood and blood analogs. In: How TV (ed) *Advances in hemodynamics and hemorheology*. JAI Press, pp 1–30
- Hockney RW, Eastwood JW (1981) *Computer simulation using particles*. McGraw-Hill, New York
- Haile PM (1992) *Molecular dynamics simulation*. Wiley, New York
- Rapaport DC (1995) *The art of molecular dynamics simulation*. Cambridge University Press, Cambridge
- Flekoy E, Coveney PV, Fabritis G (2000) *Phys Rev E* 62:2140–2157
- Angenbaum JM, Peskin CS (1985) *J Comput Phys* 14:177–198
- Hoogerbrugge PJ, Koelman JMVA (1992) *Europhys Lett* 19:155–160
- Dzwiniel W, Yuen DA (2000) *J Colloid Interface Sci* 225:179–190
- Marsh C, Backx G, Ernst MH (1997) *Phys Rev E* 56:1976–1990
- de Groot SR, Mazur P (1962) *Non-equilibrium thermodynamics*. North-Holland, Amsterdam
- Espanol P, Serrano M (1999) *Phys Rev E* 59:6340–7
- Dzwiniel W, Yuen DA (2000) *Int J Mod Phys C* 11:1–25

50. Groisman A, Steinberg V (2000) *Nature* 405:53–55
51. Verlet L, *Phys Rev* (1967) 159:98–102
52. Gibson J, Chen K, Chynoweth S (1999) *Int J Mod Phys C* 10:241–252
53. Vattulinen I, Kartunen M, Bsold B, Polson JM (2002) *J Chem Phys* 116:3967–3979
54. Boryczko K, Dzwinel W, Yuen DA (2002) *Concurrency Pract Ex* 14:137–161
55. Amira, v. 2.3 - Advanced 3D visualization and volume modeling (2001) <http://www.amiravis.com>
56. Boryczko K, Dzwinel W, Yuen DA (2002) *Concurrency Pract Ex* 14 (in press)
57. Dzwinel W, Boryczko K, Yuen DA (2002) *J Colloid Interface Sci* (in press)
58. <http://www.cis.tugraz.at/matd/work/blood.html>
59. Prabhu RD, Hitt DL, Eggleton CD (2001) Wavelet analysis of red blood cell aggregate structures. In: *Proceedings of the 2001 ASME Bioengineering Conference*. American Society of Mechanical Engineers, New York
60. Serrano M, Español P (2001) *Phys Rev E* 64(4):4615/1–18